X-622-75-123
PREPRINT

MARTIAN ATMOSPHERIC LEE WAVES

JOSEPH A. PIRRAGLIA

MAY 1975

GSFC
GODDARD SPACE FLIGHT CENTER
GREENBELT, MARYLAND

CONTENTS

ILLUSTRATIONS

MARTIAN ATMOSPHERIC LEE WAVES

Joseph A. Pirraglia
Laboratory for Planetary Atmospheres

GODDARD SPACE FLIGHT CENTER
Greenbelt, Maryland

MARTIAN ATMOSPHERIC LEE WAVES

Joseph A. Pirraglia
Laboratory for Planetary Atmospheres
Goddard Space Flight Center
Greenbelt, Maryland 20770

ABSTRACT

The Mariner 9 television pictures of Mars showed areas of extensive mountain lee wave phenomenon in the northern mid-latitudes during winter. In most cases the characteristic wave length of the lee waves is readily observable and in a few cases the boundaries of the wave patterns, as well as the wave length, are observed. The cloud patterns resulting from the waves generated by the flow across a mountain or crater are dependent upon the velocity profile of the air stream and the vertical stability of the atmosphere. Using the stability as inferred by the temperature structure obtained from the infrared spectrometer data, a two layer velocity model of the air stream is used in calculations based on the theory of mountain lee waves. The parameters that yield a pattern similar to that in a picture with a well defined wave configuration are a lower 11 km deep air stream of 40 m/sec and an upper air stream of 85 m/sec. This calculation appears to be an upper limit of the wind speeds, with most of the pictures implying wind speeds of the lower layer to be less than 40 m/sec. These results yield magnitudes generally in agreement with circulation models, in particular, the Leovy and Mintz (1969, J. Atmos. Sci., 26, 1167) two layer numerical model. Under not too different conditions they calculate winds of approximately 30 and 70 m/sec in the lower and upper layers respectively.

MARTIAN ATMOSPHERIC LEE WAVES

INTRODUCTION

Atmospheric waves in the lee of mountains are an often observed and fairly well understood phenomena. The theory of mountain lee waves has been discussed in a series of papers by Scorer (1949, 1953, 1954), among others, and in particular for an isolated peak by Scorer (1956) and Scorer and Wilkinson (1956). Observation of this familiar terrestrial phenomenon on another planet, as was the case during the Mariner 9 mission, greatly aids in the interpretation of the data.

One of the objectives of the Mariner 9 mission to Mars was the investigation of the atmospheric thermal and dynamical behavior. The thermal structure was obtained for extensive, though not complete, coverage in local time and latitude in the earlier part of the mission and for somewhat less extensive coverage in the latter part of the mission (Hanel, et al., 1972; Conrath, et al., 1973). The dynamical nature of the atmosphere can be investigated using the thermal structure or can be inferred from apparent cloud motions (Briggs and Leovy, 1974). However, when the temperature data is supplemented by an additional observable, in particular, cloud patterns as in lee waves, winds can be inferred within the constraints imposed by the problem and serve as bounds on independently derived motion. This approach is discussed briefly by Briggs and Leovy (1974) and is the problem which will be addressed here.

During revolutions 179 to 220 of Mars the spacecraft was able to view the northern mid-latitudes during late winter. The pictures obtained during that period showed extensive waves in the clouds that comprise the edge of the polar hood (see Briggs and Leovy for a collection of cloud pictures). In many instances the cloud formations were obviously associated with atmospheric waves in the lee of mountains or craters. While these waves may be of no great consequence in the global circulation they do serve as a diagnostic means of determining wind velocities. We shall consider two examples of wave patterns and attempt to determine the airstreams which, when used in calculations based on the theory of mountain lee waves with the vertical stability as inferred by the thermal structure, yield wave patterns similar to those observed. We shall sketch the development of Scorer, repeating parts with minor modifications for continuity. A simple extension of Scorer's analysis will be used to introduce effects due to the horizontal dimensions of the crater generating the wave patterns. Rather than trying to reproduce the cloud patterns by calculating the vertical motions and condensation we shall calculate only the surfaces of constant phase. The wave patterns will be inferred by considering sections along the wave crest where the wave amplitude exceeds some reasonable but arbitrary prescribed value.

In most of the pictures the only easily observable parameter of the wave pattern is the wave length. While the whole pattern is needed to define the airstream profile the wave length alone does permit the establishment of

limits on the airstream near the surface. This will become apparent in the course of our exposition.

It will be shown that there is agreement between the observations and theory and that in the latitudes, local time and season of the observations the theory does not suggest supersonic winds as might be inferred by the cloud patterns observed in some cases.

FREE MODES OF STATIONARY WAVES

The lee wave pattern is due to the discrete spectrum of waves generated by a crater ridge in an airstream. The discrete spectrum is the set of eigenmodes whose wavenumbers are the solutions to the zero frequency dispersion equation which is derived from the homogeneous equation for the airstream.

The free modes are infinite in lateral extent, being the type of wave generated by an infinitely long ridge not necessarily normal to the airstream. A lee wave pattern of a crater is obtained by summing over a parallel set of ridges oriented at all angles between $\pm\pi/2$ from the normal to the airstream. Relative amplitudes of the modes are obtained by expanding a ridge in terms of the stationary waves with the ridge acting as a forcing function. The method is identical to a Green's function approach in which the ridge is used as the source term.

The velocity, density, entropy and acoustic velocity of an undisturbed airstream are designated by u_0, ρ_0, η_0 and c_0 respectively. Using the approach of

Eckart (1960) the parameters associated with the kinematics and dynamics of the atmosphere are defined by

$$\text{(a)}\quad \Gamma = \frac{1}{2}\frac{(\rho_0 c_0)'}{\rho_0 c_0} + \frac{g}{c_0 T}$$

$$\text{(b)}\quad N^2 = \frac{\gamma-1}{\gamma}\frac{g}{R}\eta_0' = g\left(\frac{T'}{T} + \frac{g}{c_p T}\right) \equiv g\beta \qquad (1)$$

where the prime indicates differentiation with respect to z. γ and R are the ratio of the specific heats and the gas constant. N is the Brunt-Väisälä frequency, Γ is a reciprocal scale height related to the adiabatic changes in the vertical direction and β is the static stability.

With the stationary wave vector and horizontal space vector defined by $\underline{k}$ and $\underline{r}$ the vertical velocity, w, of a stationary wave is defined by

$$w = W(\rho_0 c_0)^{-\frac{1}{2}} \exp\left[\underline{i}\,\underline{k}\cdot\underline{r}\,\frac{1}{2}\int_0^z \Gamma dx\right], \qquad (2)$$

and assuming the acoustic velocity to be greater than the stream velocity, the homogeneous equation for W is

$$W'' + \left(\frac{N^2\,|\underline{k}|^2}{|\underline{k}\cdot\underline{u}_0|^2} - |\underline{k}|^2 - \frac{\underline{k}\cdot\underline{u}_0''}{\underline{k}\cdot\underline{u}_0} - \frac{\underline{k}\cdot\underline{u}_0'}{\underline{k}\cdot\underline{u}_0}\Gamma + \frac{\Gamma'}{2} - \frac{\Gamma^2}{4}\right) W = 0. \qquad (3)$$

To obtain (3) it has also been assumed that the Rossby number is large and that the perturbation velocity of the stream is small compared to the stream velocity.

One of the simplest models, and the one that we shall use, is a two layer model in which the velocity is uniform within a layer and in the same direction

in both layers. The density decreases exponentially with altitude, the Brunt-Väisälä frequency is constant and both are continuous across the interface of the two layers. In addition, for the thermal structure of the atmosphere in which we are interested, the fifth and sixth terms are much smaller than the first term in the brackets of (3) and may be neglected. Using the subscripts 1 and 2 to identify quantities in the lower and upper layers respectively, taking the interface at $z = 0$, the surface at $z = -h$ and letting ϕ represent the angle between the wave vector and stream direction we have from (3)

$$\text{(a)} \qquad W_1'' + \left(\frac{N^2}{u_{01}^2} \sec^2 \phi - k^2 \right) W_1 = 0 \quad ; \quad 0 > Z > -h$$

$$\text{(b)} \qquad W_2'' + \left(\frac{N^2}{u_{02}^2} \sec^2 \phi - k^2 \right) W_2 = 0 \quad ; \quad z \geq 0 \tag{4}$$

The interface conditions are

$$\text{(a)} \qquad u_{01} W_1' = u_{02} W_2'$$

$$\text{(b)} \qquad \frac{W_1}{u_{01}} = \frac{W_2}{u_{02}} \tag{5}$$

and at the surface the boundary condition is

$$W_1 (-h) = 0. \tag{6}$$

Solving the set (4), (5) and (6) under the condition that the wave energy decreases with height, that is the waves are trapped (Corby and Sawyer, 1958; Scorer, 1949), the eigenvalue equation for the wave numbers k is obtained,

$$\nu \cot(\nu h) + \left(\frac{u_{02}}{u_{01}}\right)^2 \mu = 0 \tag{7}$$

where

$$\text{(a)} \qquad \nu^2 = \frac{N^2 \sec^2\phi}{u_{01}^2} - k^2 = l_1^2 - k^2$$

$$\text{(b)} \qquad \mu^2 = k^2 - \frac{N^2 \sec^2\phi}{u_{02}^2} = k^2 - l_1^2 . \tag{8}$$

The Scorer parameters l_1 and l_2 are the limits of the possible values of k. Solutions of (7) give the values of the wavenumber k_r of the free modes of the airstream.

The roots k_r define the modes of the stationary waves with wave vectors at an angle ϕ to the direction of the airstream. The modes have the horizontal behavior,

$$w \sim e^{ik_r(x\cos\phi + y\sin\phi)} \tag{9}$$

where x is in the direction of the airstream and y is normal to the airstream. If the waves are assumed to be generated by a ridge at an angle ϕ to the stream and at a distance d from the origin of the x-y plane, as shown in Fig. 1, we have,

$$w \sim e^{ik_r[r\cos(\theta - \phi) + d]} \equiv e^{ik_r\xi} \tag{10}$$

with r and θ as shown in Fig. 1.

Solutions of the form (10) represent the free modes but in order to determine the amplitudes the source of the waves must be considered. In addition, we are interested in the vertical excursion of an atmospheric parcel not its vertical velocity since the clouds will presumably form or be more dense along the crests of the waves in the streamlines. The vertical excursion, ζ_k, of a streamline for the wave of wavenumber K is related to the vertical velocity by

$$\zeta_k(z,\xi) = \frac{w}{iku_0} e^{ik\xi} \tag{11}$$

to within a constant phase parameter. The ridge is described in terms of the stationary waves by

$$\zeta_s(\xi) = a\left(1 + \frac{\xi^2}{b^2}\right)^{-1/2} = \frac{ab}{\pi} \text{ Real part } \int_0^\infty e^{-kb + ik\xi}\, dk. \tag{12}$$

Normalizing ζ_k to the amplitude of the displacement at the surface and using this with (12) which represents the boundary condition at z = -h when a ridge is in the airstream we have, with Re designating the real part,

$$\zeta_\phi(z,r,\theta) = \frac{ab}{\pi} \frac{u_0(-h)}{u_0(z)} \frac{\rho_0(z)}{\rho_0(-h)} \exp\left(\frac{1}{2}\int_{-h}^{z} \Gamma dz\right) \text{Re} \int_0^\infty \frac{W(z)}{W(-h)} e^{-kb+ik\xi} dk. \tag{13}$$

ζ_ϕ represents the vertical displacement of a streamline due to the stationary waves with wave vectors perpendicular to the ridge and at an angle ϕ to the airstream as shown in Figure 1.

If we now take

$$\begin{aligned} &(a) \qquad \xi_w = r\cos(\theta - \phi) + d \\ &(b) \qquad \xi_L = r\cos(\theta - \phi) - d \end{aligned} \tag{14}$$

$$A = ab\,[\rho_0(z)/\rho_0(-h)]\,\exp\left(\frac{1}{2}\int_{-h}^{z}\Gamma dz\right), \tag{15}$$

consider a set of parallel ridges separated by 2d, and integrate (13) over ϕ from $-\frac{\pi}{2}$ to $\frac{\pi}{2}$ we have

$$\zeta(z,r,\theta) = \frac{A}{\pi}\,\frac{u_0(-h)}{u_0(z)}\int_{-\frac{\pi}{2}}^{\frac{\pi}{2}} d\phi \int_0^\infty dk\,\frac{W(z)}{W(-h)}\;e^{-kb}\left(e^{ik\xi_w} + e^{ik\xi_L}\right) \tag{16}$$

where $\zeta(z, r, \theta)$ represents the complete solution for the displacement of the streamlines of flow across a crater. The discrete free modes represented by the solutions to (7) are at the poles of the integrand. Integration in the complex k-plane is chosen so that the waves are downstream from the crater, the integration paths being different depending upon whether ξ_w or ξ_L are less than or greater than zero. (See Scorer, 1949, for a more detailed discussion of the k-plane integration.) Evaluation of the lee waves is straight-forward and is simply the residue of the poles;

$$\zeta(z,r,\theta) = 2iA \frac{u_{01}}{u_{0j}} \int_{-\frac{\pi}{2}}^{\frac{\pi}{2}} d\phi \sum_r \frac{W_j}{\left.\frac{\partial W_1}{\partial k}\right|_{k=k_r}} e^{-k_r b} \left(e^{ik_r \xi_w} + e^{ik_r \xi_L}\right) \tag{17}$$

where $j = 1$ when $-h < z < 0$ and $j = 2$ when $z \geq 0$.

Because of the $e^{-k_r b}$ term the mode with the smallest root will be dominant and we shall consider it only and drop the summation and the r-subscript.

Separating the integral into parts containing ξ_w and ξ_L the integral is evaluated by the method of stationary phase where the stationary points ϕ_w and ϕ_L are defined by

$$\begin{aligned} &(a) \quad \frac{\partial}{\partial \phi} (k\xi_w) = 0 \\ &(b) \quad \frac{\partial}{\partial \phi} (k\xi_L) = 0 \end{aligned} \tag{18}$$

On constant phase surfaces defined by the constant M,

$$\begin{aligned} &(a) \quad k\xi_w = M \\ &(b) \quad k\xi_L = M \ . \end{aligned} \tag{19}$$

Using (18) and (19) equations are obtained for θ and r in terms of the stationary points ϕ_w and ϕ_L;

$$\tan(\theta - \phi_{w,L}) = -\frac{1}{k} \frac{\partial k}{\partial \phi} \frac{M}{M \mp dk} \tag{20}$$

$$r_{w,L} = \frac{M \mp dk}{k \cos(\theta - \phi_{w,L})} \tag{21}$$

where $(1/k)\,\partial k/\partial\phi$ is obtained from the dispersion equation (7) and the upper and lower signs are associated with the W and L subscripts respectively. Equations (20) and (21) yield r and along constant phase fonts where the phrase is determined by the constant M.

The stationary phase evaluation of (17) gives the result

$$\zeta(z, r(\phi_s), \theta(\phi_s)) = 2iA \frac{u_{0l}}{u_{0j}} \left| \frac{W_j}{\frac{\partial W_j}{\partial k}} \right|_{k=k_r} e^{-k_r b} \left\{ \left[\frac{2\pi}{\frac{\partial^2}{\partial\phi^2}(k_r \xi_w)} \right]^{1/2} e^{ik_r \xi_w \pm i\frac{\pi}{4}} + \left[\frac{2\pi}{\frac{\partial^2}{\partial\phi^2}(k_r \xi_L)} \right]^{1/2} e^{ik_r \xi_L \pm \frac{\pi}{4}} \right\} \tag{22}$$

where all the terms are evaluated at the stationary point ϕ_s, which equals ϕ_w or ϕ_L depending upon whether the wave is due to the windward or leeward rim of the crater and the sign of $\pi/4$ is + or - depending upon whether $\frac{\partial^2}{\partial\phi^2}(k\xi_{w,L})$ is greater than or less than zero. When the second derivative is equal to zero (22) is singular and the solution is similar to (22) but with the curly bracketed term replaced by

$$\left\{ 2\Gamma\left(\frac{4}{3}\right) \left[\frac{6}{\frac{\partial^3}{\partial\phi^3}(k\xi_w)} \right]^{1/3} e^{ik\xi_w + i\frac{\pi}{6}} + 2\Gamma\left(\frac{4}{3}\right) \left[\frac{6}{\frac{\partial^3}{\partial\phi^3}(k\xi_z)} \right]^{1/3} e^{ik\xi_L + i\frac{\pi}{6}} \right\}$$

with $\Gamma(4/3)$ being the gamma function.

If for $\partial^2(k\xi_{w,L})/\partial\phi^2 > 0$ we take $M = (6 + 8n - 1)\frac{\pi}{4}$ and for $\partial^2(k\xi_{w,L})/\partial\phi^2 \leq 0$ take $M = (6 + 8n + 1)\frac{\pi}{4}$ with $n = 0, 1, 2, \text{---}$, the constant phase surfaces are alternately the wave crests due to the windward and leeward rims of the crater. Using (20), (21) and (22) the amplitude and coordinates of the wave crests can be calculated as a function of ϕ_s.

DISCUSSION OF OBSERVATIONS AND CALCULATIONS

The vertical displacement of the stream lines in addition to being dependent upon the stream parameters also depend upon the parameters a and b which describe the crater ridge, as is evident in (15) and (22). As pointed out previously, to determine the wave pattern it is not necessary to calculate the wave amplitudes over the total wave field but all that is needed is the contours of the wave crests since the clouds will form initially and be most dense along a crest. If the height and slope of the ridge is assumed to be small enough to satisfy the condition that the perturbation velocity is small as compared to the stream velocity then the horizontal contours of the wave crests are independent of the vertical scales of the crater ridge leaving only the easily observable crater diameter, in addition to the airstream parameters, needed to determine a wave crest pattern. However, the width of the ridge as compared to the wave number does have an influence on the observed details of the cloud pattern. The factor e^{-kb} in (22) depends upon the angle between the airstream and the normal to the crater at its point of maximum contribution to the wave. This implies that the

ridge width determines, to some extent, the sections along the crest where the amplitude exceeds that required to cause condensation of the clouds. Thus, the location of the clouds along a wave crest is somewhat dependent upon the ridge width.

Figure 2 shows a Mariner 9 television picture taken during the 185th revolution of the planet by the spacecraft. The 100 km dia. frost coated crater in the lower left corner is at 55N latitude and 145W longitude, and the evening terminator runs across the upper left corner of the picture. At the time of the picture the subsolar latitude was 7°S, making it late winter in the northern hemisphere. The clouds in the picture are composed of water ice and are along the edge of the north polar hood which was receding at that time. (The discovery of H_2O ice clouds in the Martian atmosphere is discussed in Curran, et al., 1973.) The apparent wind direction is along the dark streak extending east of the crater. Two sets of overlapping waves can be seen in the southern part of the wave system generated by the crater where it is relatively free of interference from other waves. There is a transverse set normal to the wind direction directly in the lee of the crater and a diverging set with crests that intersect directly behind the crater. The waves fill a wedge shaped region whose edge makes an angle of approximately 18° with the apparent wind direction and the wave length of the transverse waves along the centerline of the pattern is approximately 60 km.

Using the model described in the previous section by assigning values to N^2, which depends upon the temperature profile, to the airstream speeds u_{01} and u_{02} and to the depth h of the lower airstream we attempt to construct the wave pattern which could generate the cloud configuration of Figure 2. Unfortunately, there is no temperature data available for the time of the picture but other data for the same latitude and local time indicates that the atmosphere was substantially subadiabatic and in fact may have had temperature inversions. As an approximate mean, in our models we shall use an isothermal atmosphere where from (1b), $\beta = \beta_{iso} \equiv g/(c_p T)$. Any stream velocities can then be considered to be normalized to the isothermal case and the velocity associated with any other value of β is obtained by multiplying the isothermal case by $(\beta/\beta_{iso})^{1/2}$.

Figure 3 shows families of airstream models as a function of wedge-angle and transverse wavelength. Part (a) of the figure is for lower layer velocities of 20 and 40 m/s and part (b) is for 30 and 50 m/s. In each part of the figure lines of constant lower layer depth and upper layer velocity are plotted. The point associated with the pattern of Figure 2 is indicated in both parts. The dotted portion of each section is the limit beyond which there is no transverse wave across the center line of the pattern. Evidently, any one of an infinite but bounded set of airstreams produce the correct angle and wavelength. An obvious one from the figure is the case with $u_{01} = 40$ m/s, $u_{02} = 85$ m/s and $h = 11$ km. Any model with u_{01} between approximately 30 and 45 m/s and with the appropriate values of u_{02} and h could satisfy the two constraints. This does not imply

a lack of uniqueness but rather that the whole contour of the wave must be matched, not only the two pieces of information contained in the wedge angle and wav engths along the centerline of the pattern. With our three parameter model we cannot expect to exactly duplicate the wave crest contour but simply choose that one which best fits the observation.

Figure 4 shows three wave patterns calculated using the method outlined in the previous section. All have identical wedge angles and wavelengths along the centerline of the pattern. The cases are, with $[u_{01}, u_{02}, h]$ representing the three parameters, [35, 83, 8], [40, 85, 11] and [45, 92, 15] as indicated. These were chosen by interpolation in Figure 3. Model [35, 83, 8] has wave crests with more curvature than those in Figure 2 and model [45, 92, 15] are too flat while [40, 85, 11] is a reasonably good reproduction. The observed patterns of Figure 2 lie between the two extreme models of Figure 4 which yield velocities without very large differences so that the gross features of the airstream would be obtained in any case.

The clouds would form along the contours of Figure 4 depending upon the shape of the ridge. Those in Figure 2 appear to be along the transverse waves of Figure 4 associated with the outer wedge, which is due to the windward ridge, and along the diverging waves of the inner wedge, which is due to the lee ridge. This suggests that the windward ridge of the crater is not as steep as the leeward ridge.

Figure 5 is an example of a less common wave pattern. This picture covers approximately the same area as Figure 2 and the cloud pattern is due to the same crater but proceeds that of Figure 2 by one Martian day. It is apparent that there is no transverse wave system. This is because waves cannot form in that direction for the conditions of the airstream at that time since, as predicted by (7), there is no solution for k when absolute values of ϕ are less than some non-zero magnitude. As before there is more than one model that will give the proper wedge angle and wavelength along some prescribed direction. In this case the angle is readily apparent but the wavelength is not and the best we can do is to match the angle and roughly approximate the wavelength along the streaks. A candidate airstream is [20, 85, 4] whose lee wave pattern is shown in Figure 6. There is a good similarity between Figures 5 and 6 especially in the first three waves in the lower part of the wake and in the characteristic streaks flaring out from the crater. The airstream of Figure 6 followed by that of Figure 4 by one day implies an upper layer of 85 m/s, uniform in time, over a lower layer of 20 m/s velocity increasing to 40 m/s, and of 4 km depth increasing to 11 km. This behavior is plausible being suggestive of lower layer growth.

The theory is essentially good only for far fields, i.e., kr large, but can in fact be used to give near field results for the free modes while ignoring the continuous part of the wave spectrum. An example of the agreement between theory and observation is indicated by Figure 7. This picture shows the first and second wave crests of the lee waves of a 45 km crater at 63N, 347W (this

picture is 200° in longitude from, and 3½ days prior to Figure 2). The theory predicts that the first crest is 5/8ths of a wavelength from the windward ridge of the crater. The wavelength between the two crests is 45 km and the distance from the windward rim to the first crest is 28 km which is in very good agreement with the theory.

Returning to Figure 3 for a moment and confining the discussion to patterns with complete transverse waves, the changing character of the wave pattern can be observed as a function of the airstream parameters. As the lower stream velocity increases the minimum depth of the layer must increase to produce patterns with complete transverse waves. For increasing lower stream depth the pattern becomes less dependent upon the upper stream velocity as, for example, along the $h = 10$ line for $u_{01} = 20$. As the difference between the upper and lower stream velocities decreases the pattern becomes less dependent upon the depth as is seen along the $u_{02} = 30$ line for $u_{01} = 20$. Both cases are intuitively evident. Of particular interest to us is the observation that for a given lower layer velocity a lower limit can be placed on the wavelength by the constraint that k cannot exceed l_1, as seen from (8). k equals l_1 where the contours of Figure 3 touch the zero wedge angle line. The limit on k is established without the aid of Figure 3 but the figure shows that for a given wavelength wide wedge angles infer small lower stream velocities. The implications of which in conjunction with the observations will be discussed subsequently.

NONUNIFORM STREAM DIRECTIONS

If the two streams of the model have different directions we have another parameter of the airstream that must be determined from the observations. Because, for the most part, we cannot even determine three parameters no attempt will be made to determine a fourth as expressed by the angle between the upper and lower streams. However, calculations showing the types of patterns that are the result of nonuniform stream directions will be presented.

If the angle between the two streams is ψ the eigenvalue equation for k is,

$$\nu \cot(\nu h) - \left(\frac{u_{01} \cos(\phi + \psi)}{u_{01} \cos \phi} \right)^2 \mu = 0 \tag{23}$$

where

$$\text{(a)} \quad \nu^2 = \frac{N^2 \sec^2 \phi}{u_{01}^2} - k^2$$

$$\text{(b)} \quad \mu^2 = k^2 - \frac{N^2 \sec^2(\phi + \psi)}{u_{02}^2} \tag{24}$$

with (23) and (24) used in the place of (7) and (8) the analysis proceeds as before.

Using a model with a lower stream velocity of 20 m/s and depth of 5 km and an upper stream velocity of 80 m/s the patterns were calculated for cases in which the angle between the streams was 45° and 90°. Similar calculations were made with a 10 km deep lower stream of 40 m/s. The results are shown in Figure 8. The calculations indicate that a pair of streams with similar depth and wind speeds will yield shorter wavelengths for larger angles between the streams. However, the observed wave patterns generally are not suggestive of

the type of patterns shown in Figure 8 and the conclusions drawn from the parallel stream case of the previous section should be valid. The streams may be off parallel but not by the amounts used for the calculations of Figure 8. If there were indications of greatly different wind directions, without observations of isolated lee wave patterns it would be exceedingly difficult to determine four parameters of the airstream.

CONCLUSIONS

Regardless of the simple model used for the airstream the calculations appear to be capable of reproducing the observed wave patterns. Insofar as the model is a reasonable approximation to the actual airstream, were it not for the paucity of temperature data at the latitude and season of the observations, accurate assessments of the wind velocities could be made. Since all our calculations were for a 200K isothermal atmosphere the velocities would have to be adjusted by the square root of the ratio of the stabilities, as was pointed out previously. If the temperature profile approached an adiabatic state the velocities as calculated would decrease toward zero. If there were a temperature inversion, the velocities would increase, but to increase the velocities by 25% over those of the isothermal case would require an inversion of more than 6K/Km. Such an inversion is large and not very likely, making the possibility of velocities greater by 25% improbable.

The first wave in the clouds shown in Figure 2 is not normal to the apparent stream direction and may be due to the nonuniformity of the wind direction with

altitude. As illustrated previously, the wave patterns are not symmetric about a horizontal line when the windstreams have different directions but the wave patterns do not suggest a large difference in the wind directions. With small differences and without isolated patterns it is not possible to determine the difference in the stream direction but, nevertheless, one may use the wavelengths to give an estimate of the winds in the lower layer.

In most of the television pictures the wavelengths of the apparent lee waves are approximately 30 km and of the type shown in Figures 2 and 4 rather than those of Figures 5 and 6. Although the lack of many clear cases of wave patterns showing the wedge angle prevents a determination of the upper airstream velocity, an upper limit can be put on the velocity of the lower stream. From Figure 3 it is apparent that wavelengths of 30 km are associated only with airstreams with lower stream velocities less than 40 m/s since the observations suggest wide wedge angles and from the discussion in the previous section they are associated with the smaller lower stream velocities for a given wavelength.

Pictures like Figure 5 give the impression of very high velocities but the results of the calculations shown in Figure 6 and compared with Figure 5 imply that there is no need to invoke extremely high velocities to explain the particular wake pattern and, in fact, the surface velocity is less than the more common cases with transverse waves.

The conclusion may be made that the many observations of lee waves suggest that the near surface wind speeds, except possibly on a very localized

scale, do not greatly exceed, and most of the time are less than, 40 m/sec in the northern midlatitudes during the late winter. This result is in agreement with the wind magnitudes obtained independently, in particular with the two level numerical model of Leovy and Mintz (1969) where they calculated the mean zonal winds at 50N and at winter solstice to be 30 m/s at 3Km and 70 m/s at 13.5 Km. Winds of this magnitude are in substantial agreement with the winds implied by the lee waves.

One may question the validity of the two layer model used to describe the wind profile. The two layer model with a discontinuous velocity profile is subject to Kelvin-Helmholtz instabilities at all wavelengths. However, a three layer model with uniform upper and lower velocities connected continuously through the varying middle layer is unstable to only a small band of wavenumbers which are dependent upon the Richardson number and any Kelvin-Helmholtz instability wavelength is likely to be far removed from the lee wave lengths. If the product of the transition layer thickness and the wavenumber is much less than unity the two layer approximation in which the transition layer is absent is a good approximation for the calculation of lee waves in a continuously varying velocity profile airstream. The only question that remains is whether or not the three layer model is an adequate representation of the airstream. The extensive periodic train of lee waves observed is the result of the waves being trapped in a waveguide formed by layers in which the Scorer parameter, $l = N \sec\phi/u_0$, allows propagation in a lower layer and reflection

in an upper layer. The three layer model is general enough to permit trapping of the waves and continuity of the velocity profile and should then be at least a rough approximation to the actual airstream and its two layer approximation is adequate for the calculation of lee waves.

ACKNOWLEDGEMENTS

The author is indebted to Dr. B. J. Conrath for his helpful discussions and to he and Dr. R. A. Hand for critical comments. The Mariner 9 MTVS photography has been provided by the National Space Science Data Center.

REFERENCES

1. Briggs, G. A. and C. B. Leovy (1974). Mariner 9 observations of the Mars north polar hood. Bull. Amer. Meteor. Soc., 55, 278-296.

2. Conrath, B., R. Curran, R. Hanel, V. Kunde, W. Maguire, J. Pearl, J. Pirraglia, and J. Weller (1973). Atmospheric and surface properties of Mars obtained by infrared spectroscopy on Mariner 9. J. Geophys. Res., 78, 4267-4278.

3. Corby, G. A.,and J. S. Sawyer (1958). The air flow over a ridge — the effects of the upper boundary and high-level conditions. Quart. J. R. Met. Soc., 84, 25-37.

4. Curran, R. J., B. J. Conrath, R. A. Hanel, V. G. Kunde, and J. C. Pearl (1973). Mars: Mariner 9 spectroscopic evidence for H_2O ice clouds. Science, 182, 381-383.

5. Eckhart, C., (1960). "Hydrodynamics of Oceans and Atmospheres." The Macmillan Co., New York.

6. Hanel, R., B. Conrath, W. Hovis, V. Kunde, P. Lowman, W. Maguire, J. Pearl, J. Pirraglia, C. Prabhakara, B. Schlachman, G. Levin, P. Straat, and T. Burke (1972). Investigation of the Martian environment by infrared spectroscopy on Mariner 9. Icarus 17, 423-442.

7. Leovy, C. and Y. Mintz (1969). Numerical simulation of the atmospheric circulation and climate of Mars. J. Atmos. Sci., 26, 1167-1190.

8. Scorer, R. S. (1949). Theory of waves in the lee of mountains. Quart. J. R. Met. Soc., 75, 41-56.

_____ (1953). Theory of airflow over mountains: II — The flow over a ridge. Quart. J. R. Met. Soc., 79, 70-83.

_____ (1954). Theory of airflow over mountains: III Airstream characteristics. Quart. J. R. Met. Soc., 80, 417-428.

_____ (1956). Airflow over an isolated hill. Quart. J. R. Met. Soc., 82, 75-81.

_____ and M. Wilkinson (1956). Waves in the lee of an isolated hill. Quart. J. R. Met. Soc., 82, 419-427.

FIGURE CAPTIONS

Figure 1. Horizontal geometry of airstream, ridge and wave directions. The ridge is at a distance d from the x-y and r-θ coordinate origin and its normal is at an angle ϕ to the airstream u_0. The wave vector $\underline{k}$ is normal to the ridge.

Figure 2. Mariner 9 television photograph taken during the 185th revolution of the planet by the spacecraft showing an extensive system of lee waves. The white circular region in the lower left corner is a frost coated 100 km diameter crater located at 55N latitude and 145W longitude. The evening terminator runs diagonally up from the lower right corner.

Figure 3. Plots of wedge angle vs. wavelength of transverse wave for various upper and lower airstream speeds and lower layer depths. Part (a) shows the two surfaces with lines of constant depth and upper stream speeds for lower stream speeds of 20 and 40 meters per sec. Part (b) shows similar surfaces for lower stream speeds of 30 and 50 meters per sec. The wavelength and wedge angle of the wave system of Figure 2 is indicated by the black circle in both parts of the figure.

Figure 4. Calculated wave patterns. Part (a) is the wave system generated by a 100 km dia. crater in an airstream with a 45 m/s, 15 km deep lower stream and a 92 m/s upper stream. Part (b) is with a 40 m/s, 11 km deep lower stream and 85 m/s upper stream. Part (c) is with a 35 m/s, 7.8 km deep lower stream and 82.5 m/s upper stream.

Figure 5. Mariner 9 television photograph taken during revolution 183. The crater on the left border is the same one shown in Figure 2. The time of this picture precedes that of Figure 2 by two Martian days and there are no transverse waves here as are evident in Figure 2.

Figure 6. The calculated wave system generated by a lower stream of 20 m/s and 3.5 km depth and an upper stream of 85 m/s blowing over a 100 km dia. crater.

Figure 7. Mariner 9 picture of two lee wave crests due the 45 km dia. crater at 63N latitude and 347W longitude.

Figure 8. Calculated wave patterns for two layer air streams in which the upper and lower velocities have different directions. The speeds, lower layer depth and angle between the velocities of the upper and lower streams are indicated in each section of the figure.

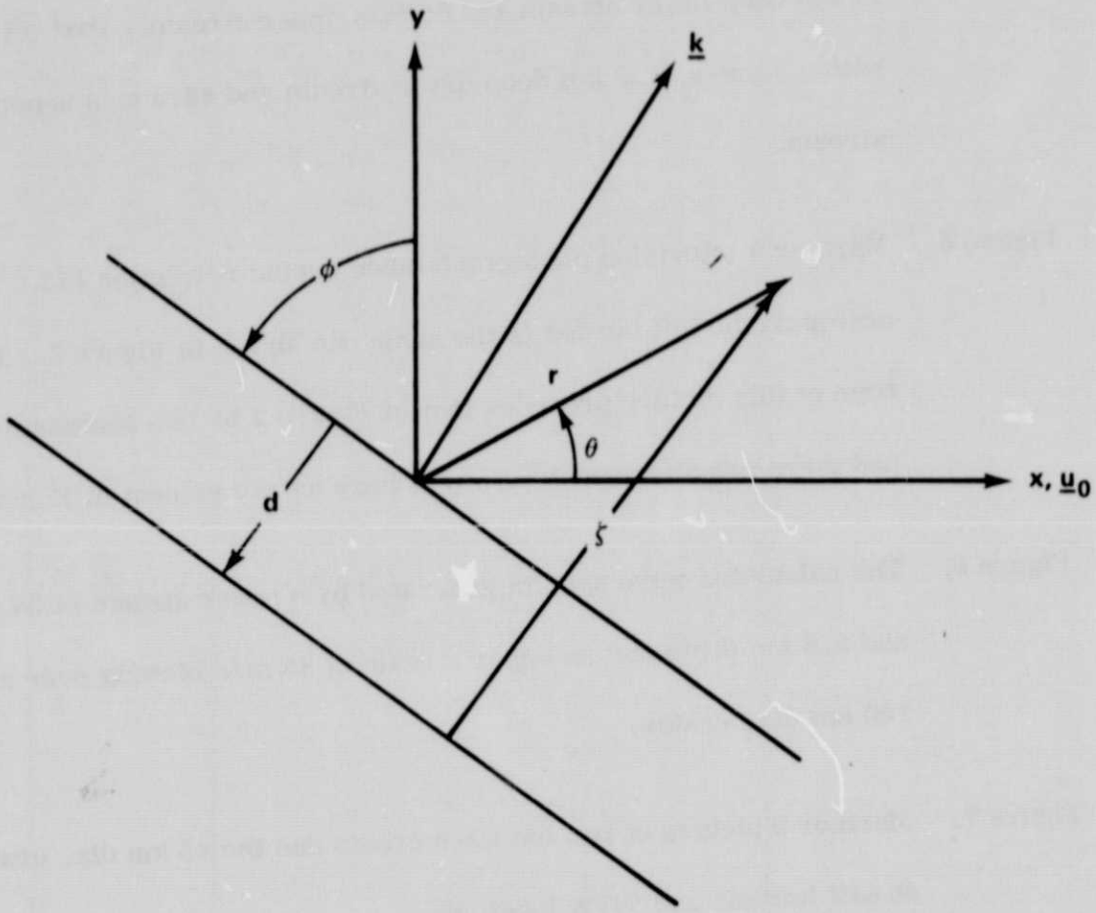

Figure 1. Horizontal geometry of airstream, ridge and wave directions. The ridge is at a distance d from the x-y and r-θ coordinate origin and its normal is at an angle ϕ to the airstream u_0. The wave vector k is normal to the ridge.

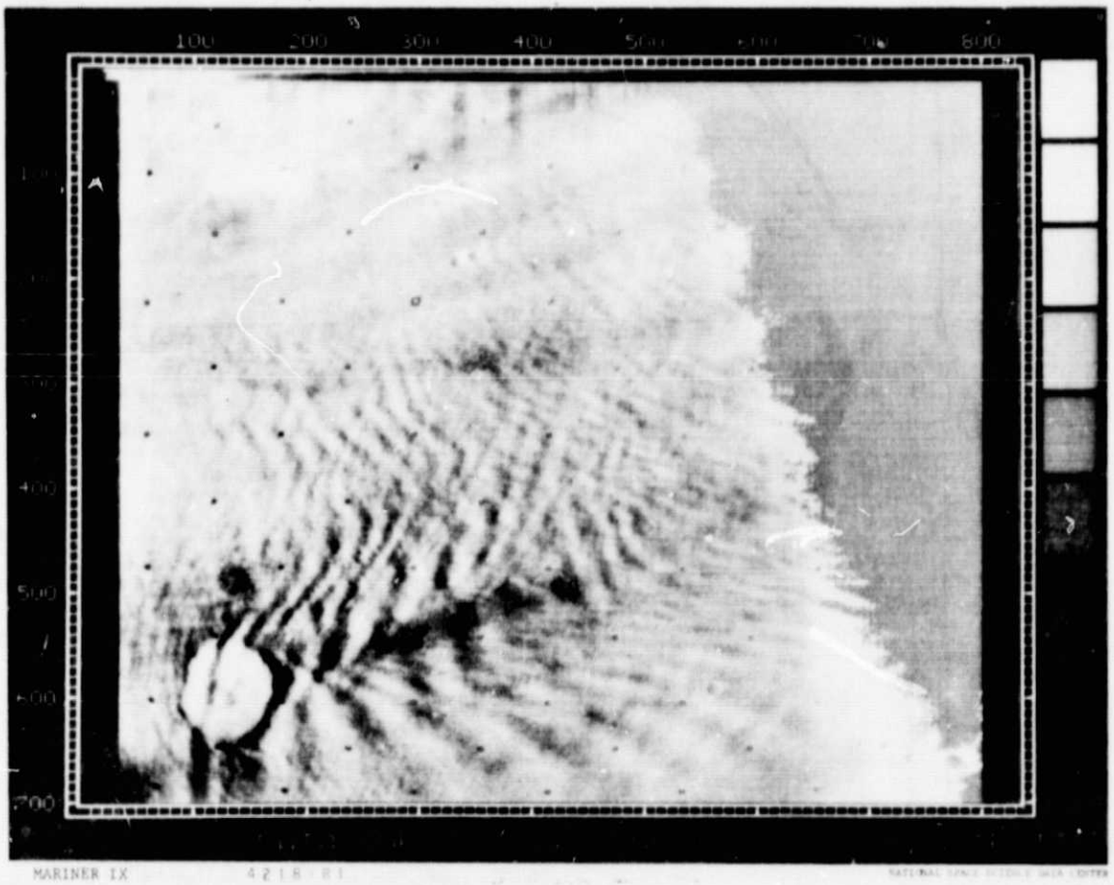

Figure 2. Mariner 9 Television Photograph Taken During the 185th Revolution of the Planet by the Spacecraft Showing an Extensive System of Lee Waves. The White Circular Region in the Lower Left Corner is a Frost Coated 100 km Diameter Crater Located at 55N Latitude and 145W Longitude. The Evening Terminator Runs Diagonally Up From the Lower Right Corner.

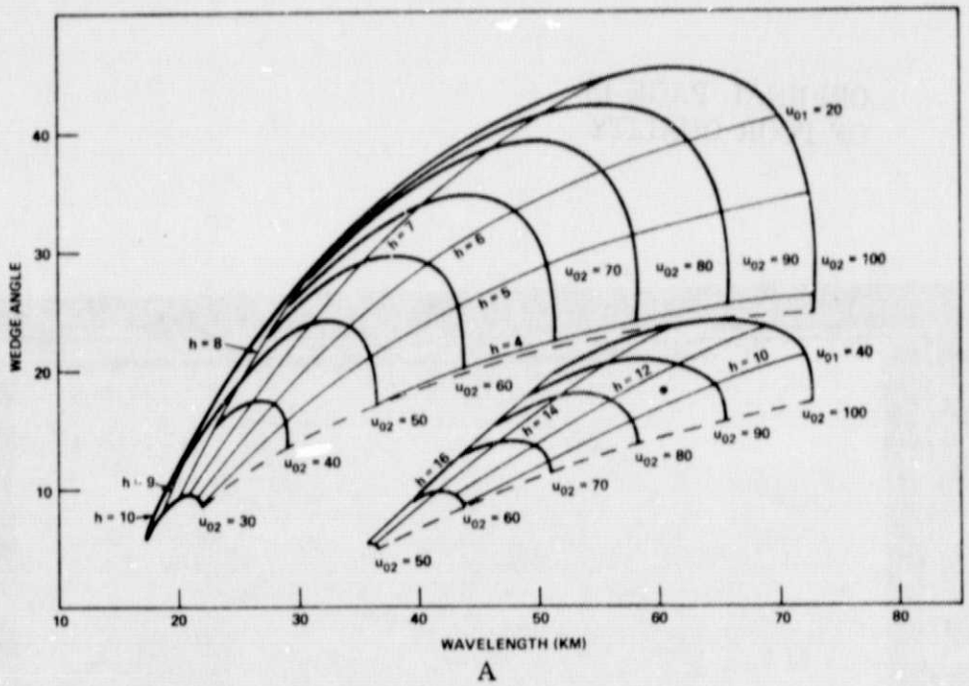

A

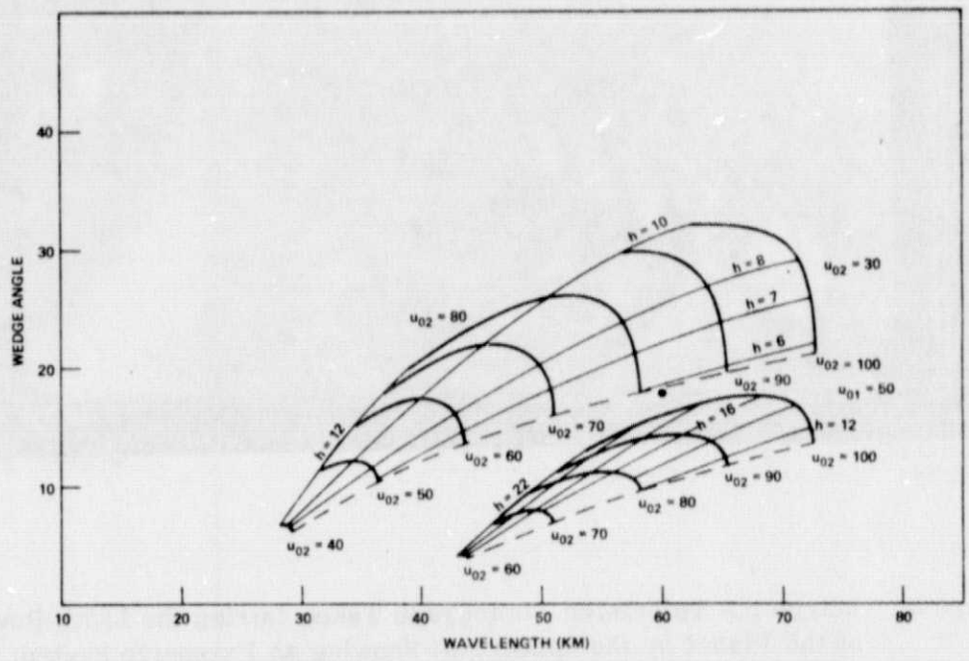

B

Figure 3. Plots of wedge angle vs. wavelength of transverse wave for various upper and lower airstream speeds and lower layer depths. Part (a) shows the two surfaces with lines of constant depth and upper stream speeds for lower stream speeds of 20 and 40 meters per sec. Part (b) shows similar surfaces for lower stream speeds of 30 and 50 meters per sec. The wavelength and wedge angle of the wave system of Figure 2 is indicated by the black circle in both parts of the figure.

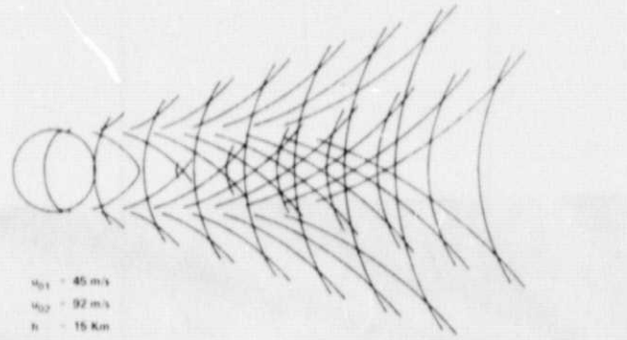

a

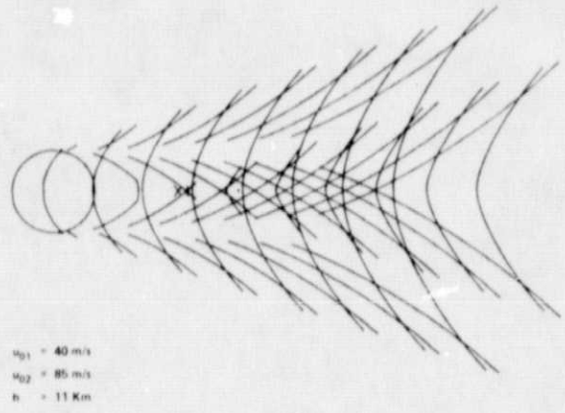

b

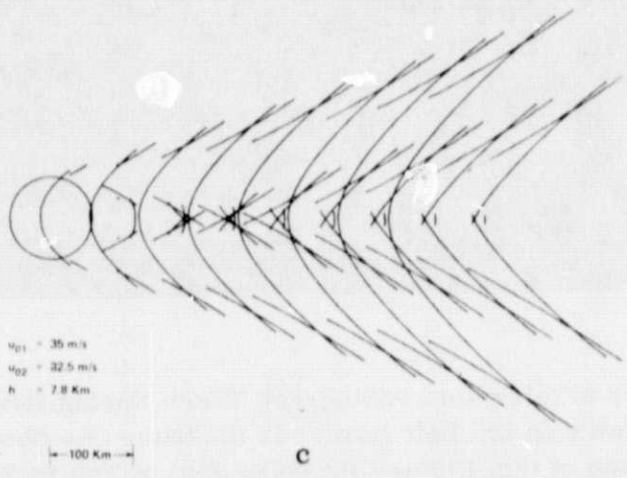

c

Figure 4. Calculated wave patterns. Part (a) is the wave system generated by a 100 km dia. crater in an airstream with a 45 m/s, 15 km deep lower stream and a 92 m/s upper stream. Part (b) is with a 40 m/s, 11 km deep lower stream and 85 m/s upper stream. Part (c) is with a 35 m/s, 7.8 km deep lower stream and 82.5 m/s upper stream.

Figure 5. Mariner 9 Television Photograph Taken During Revolution 183. The Crater on the Left Border is the Same One Shown in Figure 2. The Time of this Picture Precedes that of Figure 2 by Two Martian Days and There are No Transverse Waves Here as are Evident in Figure 2.

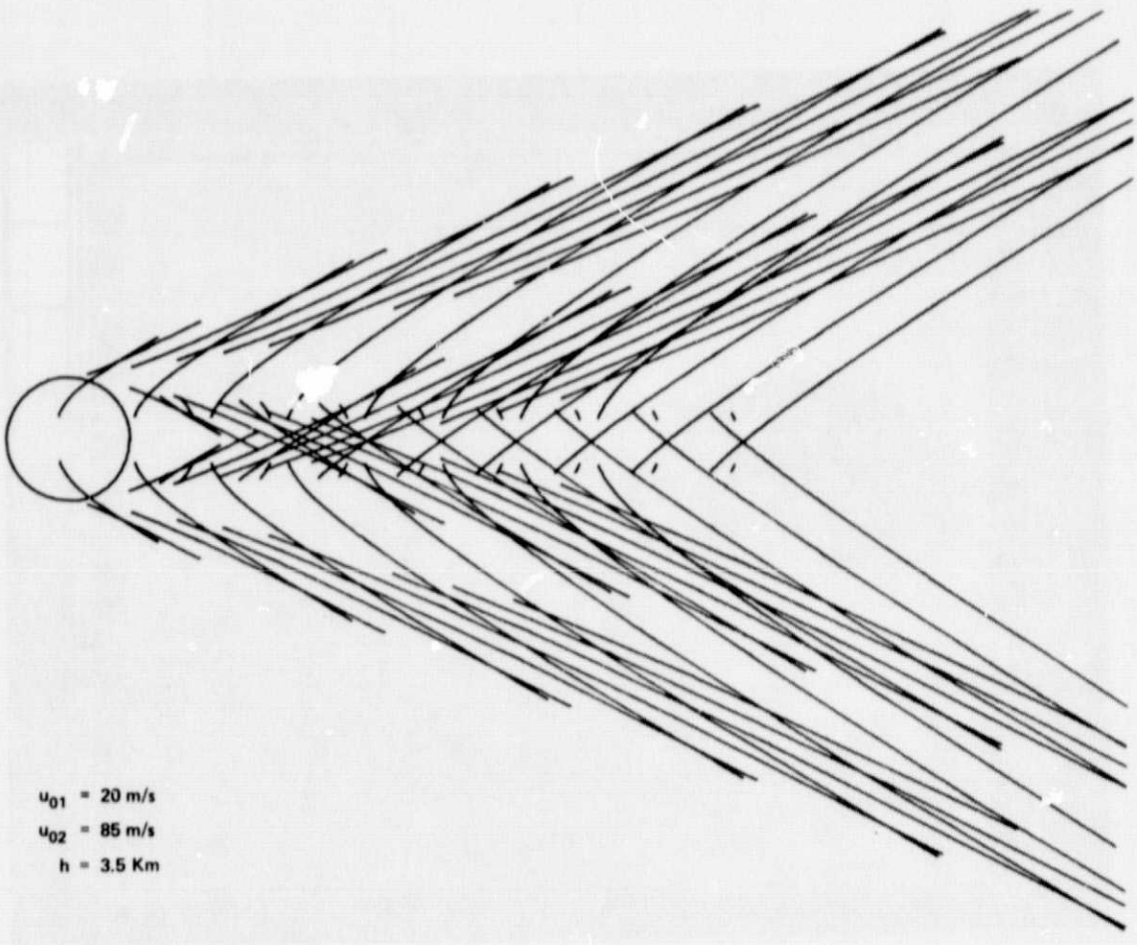

Figure 6. The calculated wave system generated by a lower stream of 20 m/s and 3.5 km depth and an upper stream of 85 m/s blowing over a 100 km dia. crater.

Figure 7. Mariner 9 Picture of Two Lee Wave Crests Due the 45 km Dia. Crater at 63N Latitude and 374W Longitude.

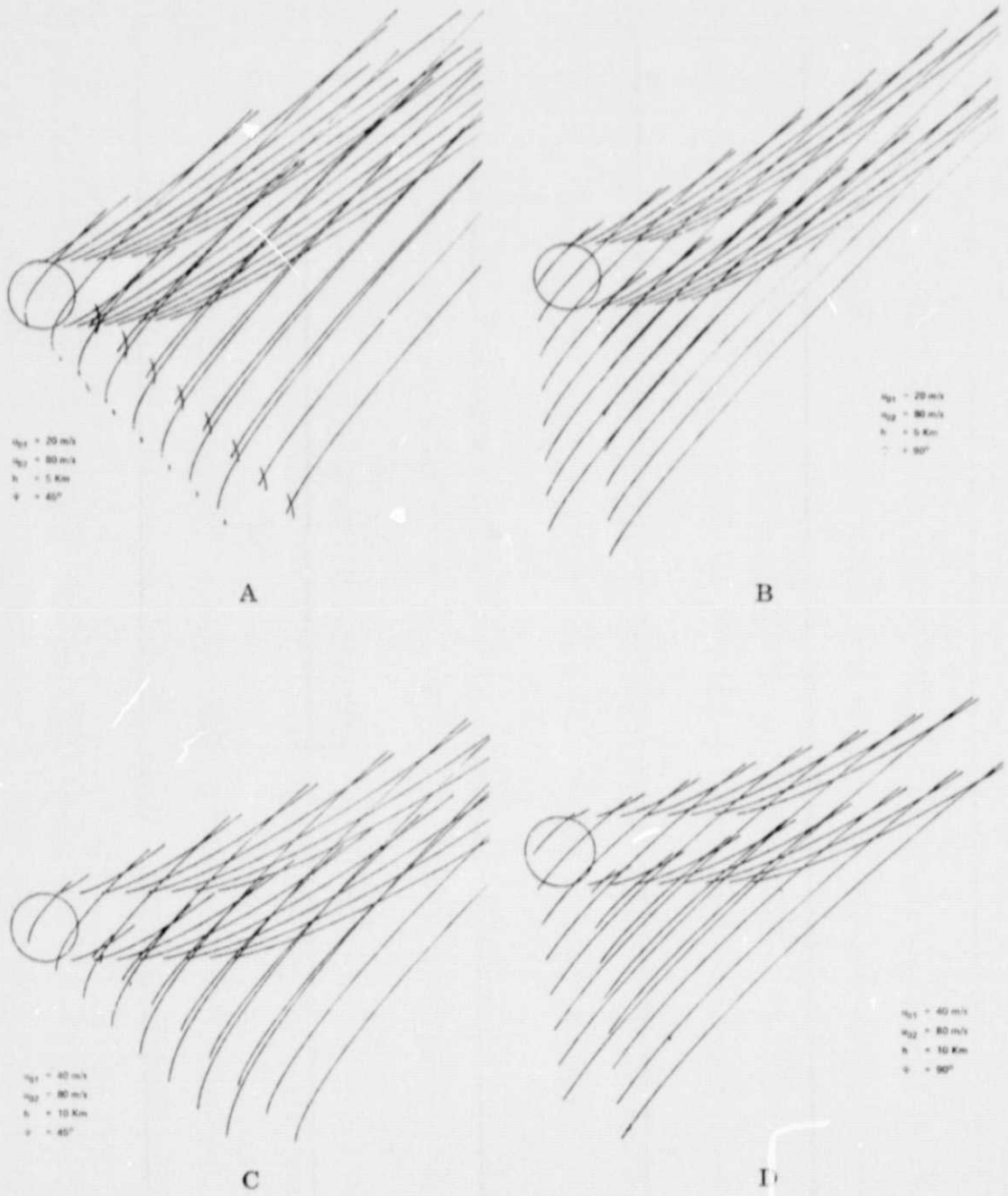

Figure 8. Calculated wave patterns for two layer air streams in which the upper and lower velocities have different directions. The speeds, lower layer depth and angle between the velocities of the upper and lower streams are indicated in each section of the figure.